ELSEVIER

Applied Catalysis B: Environmental 16 (1998) 127–138

APPLIED CATALYSIS B: ENVIRONMENTAL

# Image simulation and experimental HREM study of the metal dispersion in $Rh/CeO_2$ catalysts. Influence of the reduction/reoxidation conditions

S. Bernal*, J.J. Calvino, M.A. Cauqui, J.A. Pérez Omil, J.M. Pintado, J.M. Rodríguez-Izquierdo

*Departamento de Ciencia de los Materiales, Ingeniería Metalúrgicay Química Inorgánica, Universidad de Cádiz, Facultad de Ciencias, Apartado 40, 11510 Puerto Real (Cádiz), Spain*

Received 15 March 1997; received in revised form 24 June 1997; accepted 6 July 1997

**Abstract**

This work reports on a high resolution electron microscopy (HREM) study of a series of $Rh/CeO_2$ catalysts prepared from both $Rh(NO_3)_3$ and $RhCl_3$ metal precursors. Our attention is focused on the influence of the reduction/reoxidation conditions on the metal particle size distribution. From the analysis of both experimental and computer simulated HREM images, we were able to conclude that the truncated cubo–octahedron model describes well the morphology of the rhodium microcrystals grown on ceria. Likewise, we have used the computer simulation techniques to estimate the lowest size limit for HREM detection of the rhodium particles in $Rh/CeO_2$ catalysts. In our case, the smallest metal particles are well above the detection limit, and therefore, the reported size distributions account well for the actual ones. Three different (A–C) size distribution curves have been built up. From their analysis, we conclude that metal dispersions estimated from the mean size metal particle ($D_d$) can significantly deviate from the more accurate values determined from the so-called type C distribution curves ($D_m$). Reduction treatments up to 973 K induce a progressive sintering of the metal, the effect becoming much stronger upon reduction at 1173 K. We have also found that metal dispersion is more sensitive to the reduction treatment in $Rh(Cl)/CeO_2$ catalysts. Among the reoxidation temperatures investigated by us, rhodium redispersion could only be observed at the highest temperatures: 1073 K or 1173 K. By contrast, reoxidation at 773 K causes significant metal sintering effects. © 1998 Elsevier Science B.V.

*Keywords:* $Rh/CeO_2$; High resolution electron microscopy; Experimental and computer simulated; Metal dispersion; Reduction/reoxidation condition

## 1. Introduction

In addition to their acknowledged interest as model systems for investigating the so-called TWC's (Three Way Catalysts) [1,2], ceria supported noble metal catalysts are being intensively studied because of their likely exhibition of strong metal/support interaction effects [3–7]. Consequently to this, the determination of the metal dispersion by procedures other than chemical techniques is particularly important. The

*Corresponding author. Fax: 34-56834924.


*PII* S0926-3373(97)00066-0

dispersion data obtained in this way would be used as a reference for those determined from chemisorption essays, thus allowing to detect the chemical perturbations inherent to the onset of the strong metal/support interaction phenomena.

A number of recent studies [8–15], some of them from our own laboratory [11–15], have clearly shown that HREM can be fruitfully applied to the nanostructural characterization of $M/CeO_2$ catalysts. In particular, it can provide detailed information about the morphology, and metal decoration effects in ceria supported rhodium catalysts [11].

In this work, we report on the results obtained for a series of $Rh/CeO_2$ catalysts prepared from both rhodium nitrate and rhodium chloride metal precursors. Our major concern will be the investigation of the influence of the reduction/reoxidation conditions on the metal particle size distribution, and, consequently to this, on the metal dispersion. This has allowed us to establish the sintering/redispersion effects induced by treatments applied in a wide range of thermal conditions. Such an information should be considered highly interesting in connection with the deactivation/regeneration mechanisms operating in TWC's. As several authors [16,17] have outlined, deactivation is a major problem to be solved in this sort of catalytic system.

## 2. Experimental

The ceria supported rhodium catalysts investigated here were prepared by the incipient wetness impregnation technique from an aqueous solutions of either $Rh(NO_3)_3$, $Rh(N)/CeO_2$, or $RhCl_3$, $Rh(Cl)/CeO_2$. The cerium dioxide, 99.9% pure, with high textural stability and low surface area, was from Alpha Ventron. After the impregnation treatment, the samples were dried in air, at 383 K, for 10 h, and further stored in a desiccator until their reduction. The impregnation/drying cycles were repeated several times up to reaching a final by weight metal loading of 2.4% for $Rh(N)/CeO_2$, and 1.9% for $Rh(Cl)/CeO_2$.

The reduction treatments were performed by heating the corresponding Metal precursor/Support system, in a flow of $H_2$ (60 $cm^3$ $min^{-1}$), from 298 K to the selected reduction temperature ($T_{redn}$: 623 K, 773 K, 973 K and 1173 K). The heating rate was always 10 K $min^{-1}$. The samples were held for 1 h at $T_{redn}$; then they were treated with flowing He for 1 h at $T_{redn}$, and finally they were cooled also in a flow of inert gas. In the specific case of the catalysts reduced at 623 K, the heating in a flow of He following the reduction treatment was performed at 773 K. In this way, we ensure the elimination of the hydrogen which is expected to remain chemisorbed on ceria after reduction at 623 K [18,19]. Reoxidation treatments were performed in flowing $O_2$ (60 $cm^3$ $min^{-1}$), at a heating rate of 10 K $min^{-1}$, from 298 K to the selected reoxidation temperature ($T_{reoxn}$). The samples were kept at $T_{reoxn}$ for 1 h, and further cooled to 298 K also in a flow of $O_2$.

The HREM images were recorded on a JEOL-2000-EX microscope with 0.21 nm point resolution. The instrument was equipped with a top-entry specimen holder and an ion pump. To prevent the fast reoxidation of the reduced catalysts to be investigated by HREM, they were cooled to 191 K, always in a flow of He, then treated with $O_2$(5%)/He for 30 min, warmed up to 295 K in the mild oxidizing mixture, and finally exposed to air. The samples thus prepared were rapidly transferred into the microscope by following the procedure reported elsewhere [15].

The computer-simulated HREM images presented in this work were obtained by running the EMS (Electron Microscopy Software) package on Silicon Graphics Workstations (INDY 4400SC or IRIS 4D35/TG+). The supercell structural models used as inputs for the computer simulations were generated by running the so-called RHODIUS program developed by us [20]. This Program, which is written in FORTRAN 77, allows us to build up large supercells consisting of a metal microcrystal grown on the ceria support. The size, shape and orientation of the metal crystallite can

Table 1
Rh and $CeO_2$ basic crystallographic data

| | Phase | |
|---|---|---|
| | Rh | $CeO_2$ |
| Crystal system space group | Cubic<br>Fm 3 m | Cubic<br>Fm 3 m |
| Lattice parameter (nm) | 0.3803 | 0.5411 |
| Assymetric unit | Rh: 0,0,0 | Ce: 0,0,0<br>O: 1/4, 1/4, 1/4 |
| Lattice spacings of interest (nm) | $d_{110}$:0.269<br>$d_{111}$: 0.219 | $d_{110}$: 0.383<br>$d_{111}$: 0.312 |

be controlled at will. Likewise, the RHODIUS program allows to define the crystallographic and chemical nature of the metal/support interface.

Table 1 summarizes some basic crystallographic data for both metallic rhodium and the cerium dioxide. They can help to a better understanding of the structural considerations made in this work.

## 3. Results and discussion

By analysing several hundreds HREM images like those shown in Fig. 1 (c) and Fig. 1 (f), we have been able to conclude that most of the metal microcrystals can be described in terms of a truncated cubo–octahedron morphology. To confirm such a proposal, computer simulated images like those reported in Fig. 1 (b) and Fig. 1 (e) were obtained. The model metal particle used in these calculations consisted of a rhodium crystallite resulting from the truncation of a whole cubo–octahedron particle at the central (111) plane. The crystallographic data used as input in our computer calculations were generated by running the so-called RHODIUS program developed at our laboratory [20]. Earlier studies [9,11] have shown the occurrence of well defined epitaxial relationships between the rhodium microcrystals and the ceria support. Specifically, we have observed [11] that most of the metal particles are oriented with respect to ceria in such a way that (111) metal planes grow parallel to (111) ceria planes. In addition to the particle morphology, our structural supercell model takes into account this characteristic feature, the metal/support interface consisting of a (111) basal plane of the metal particle seating on a ceria surface with the same Miller indexes. Fig. 1 (a) and Fig. 1 (d) account for views of the supercell model along (110) and close to (100) directions, respectively.

As deduced from the comparison of both experimental and simulated images, the proposed morphology for the rhodium microcrystals leads to computer calculated HREM images in good agreement with the shape of those recorded in the microscope. Our proposal is also consistent with the experimental HREM micrographs reported in the literature for a number of $M/CeO_2$ (M: Rh, Pt) catalysts [8–15], as well as for noble metal microcrystals evaporated on some inert substrates [21].

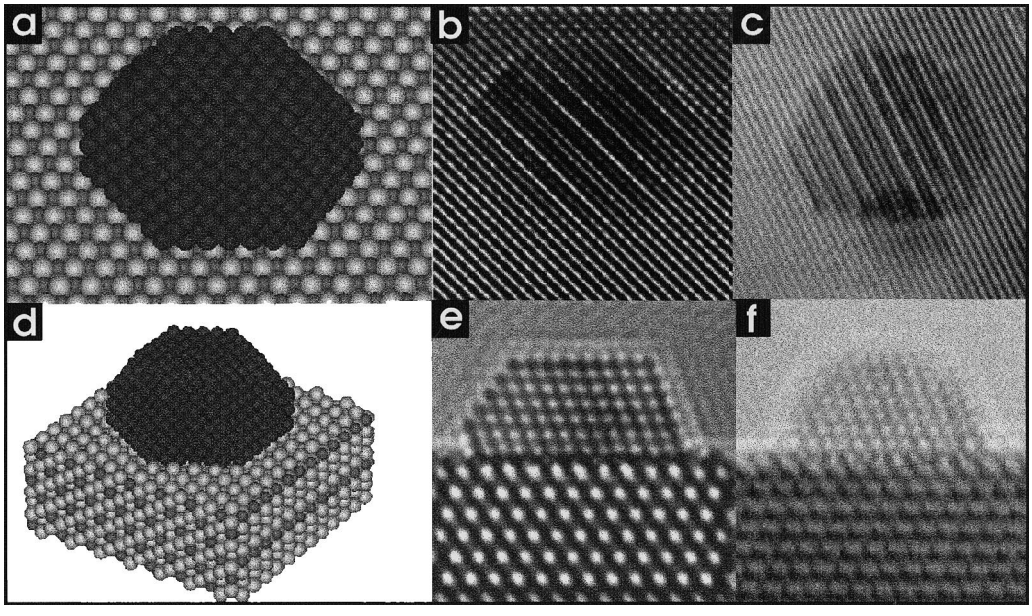


Fig. 1. Comparison between experimental (c and f) and computer simulated (b and e) HREM images for $Rh/CeO_2$ in planar (c and d) and profile (f and e) views. The supercell structural model used as the input for the computer calculations are shown in a (Rh zone axis [100]) and d (Rh zone axis: [110]).

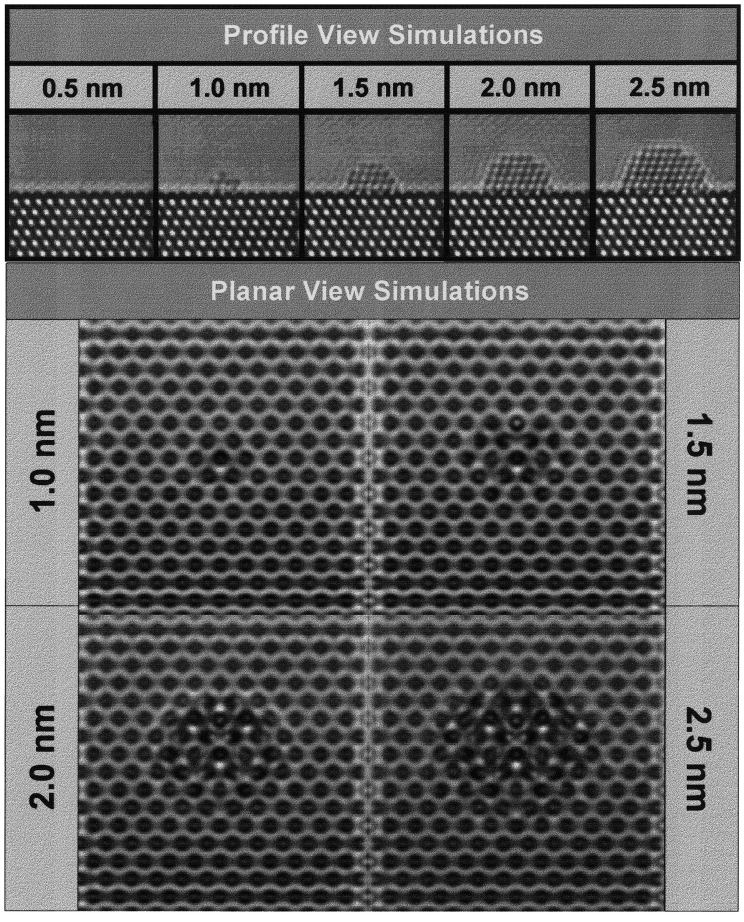


Fig. 2. Computer simulation study of the detection limit for rhodium particles supported on ceria: profile view (upper part) and planar projection (bottom). Simulation conditions: accelerating voltage: 200 kV; Cs: 0.7 mm; aperture diameter: 10 $nm^{-1}$; $\Delta$f: 50 nm; defocus spread: 10 nm; beam semiconvergence: 1.2 mrad; support thickness: 10 nm; metal/support orientation relationship: parallel indexes.

A second important question deals with the detection limit for rhodium microcrystals dispersed on ceria. Computer simulation techniques are also very useful in this respect. By using the structural model described in Fig. 1 (d), we have just modified the metal microcrystal size and calculated the corresponding profile, and planar projection images, Fig. 2. Metal particles ranging from 1 rhodium atom to 3 nm were considered. Though the results obtained from the computer simulation are sensitive to specific electron–optical conditions as well as to the ceria thickness, our previous experience [11] suggests that the selected ones can give us a reasonable idea of the searched limit. As deduced from both planar projection and profile calculated images, such a limit is around 1 nm. Some metal particles close to this threshold size have been marked by black arrows in Fig. 4. Accordingly, we conclude that, for catalysts exhibiting mean/low metal dispersions, as is the case of those investigated here, the distribution curves determined by using HREM fully account for the actual ones.

In a recent computer simulation study [22], it has been shown that the HREM image formation process can induce an apparent relaxation on the atom positions near the edges of metal particles, thus leading to an apparent enlargement of the particle size. In Ref. [22], the analysis was performed on isolated nanoparticles; accordingly, it seemed interesting to us the

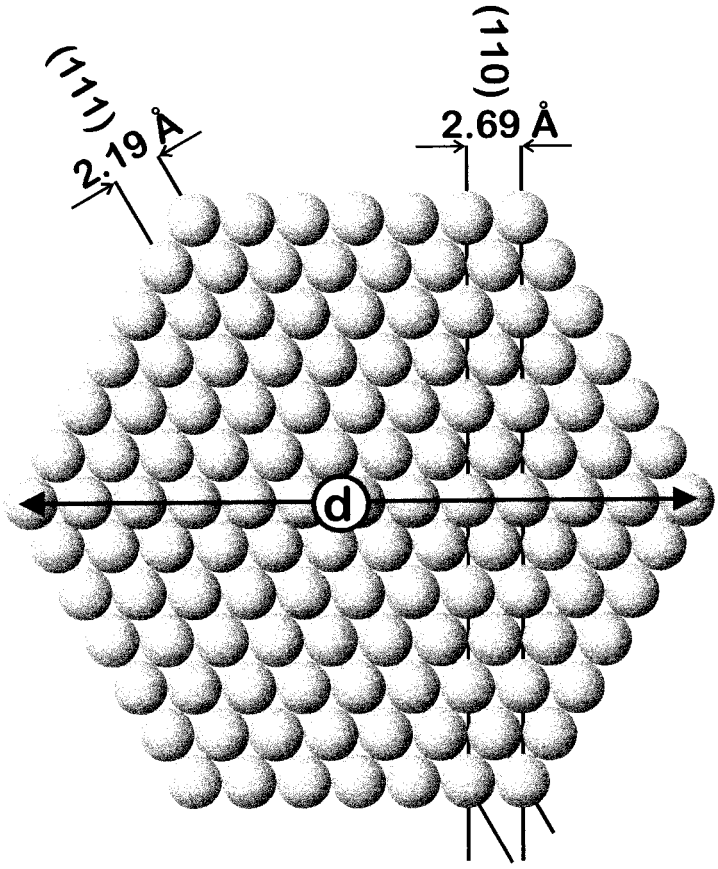


Fig. 3. (111) basal plane of the truncated cubo–octahedron model particle.

application of the computer simulation techniques to the evaluation of the apparent distortion effects induced on the metal particle size in $Rh/CeO_2$ catalysts. Upon comparison of the values determined by digital processing of the simulated HREM images with those of the model particles used as the basis for the computer calculations, we have found that the distortions do occur, but they are below the experimental error of the size measurement. Therefore, we can conclude that, for the nanosized ceria supported rhodium particles investigated here, this effect does not disturb our measurements significantly.

Fig. 3 shows the (111) basal plane of the truncated cubo-octahedron rhodium particle used as a model in the present study. The distance marked with $d$ on Fig. 3 will be used as a measurement of the particle size. The following relationship between $d$ and the number of atoms on the edges of the (100) faces of the cubo–octahedron, $m$, can be easily established:

$$d = (3m - 2)d_{110} \quad (1)$$

where $d_{(110)}$ represents the (110) metal lattice spacing, 0.272 nm in the case of rhodium. The parameter $m$ is that used by Van Hardeveld and Hartog [23] to measure the size of the cubo–octahedron metal particle, and should not be confused with the number of atoms along the edges delimiting the basal plane of the metal particle.

In Ref. [23], Van Hardeveld and Hartog have also developed equations allowing to estimate the total number of metal atoms, $N_t$, as well as the number of surface atoms, $N_s$, associated to a particle with defined morphology and size. As already stated, the model particle proposed in this work corresponds to a

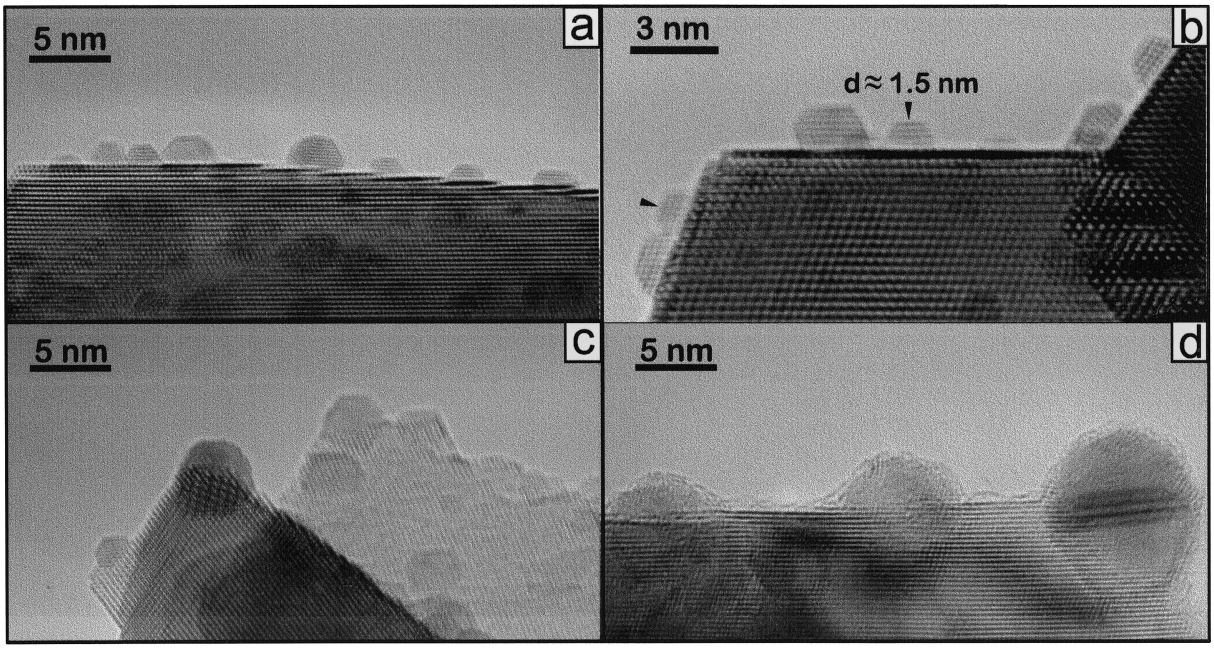


Fig. 4. HREM micrographs corresponding to $Rh/CeO_2$ catalysts reduced at 623 K (a), 773 K (b), 973 K (c) and 1173 K (d). (a), (c) and (d) images were recorded from the $Rh(N)/CeO_2$ sample, whereas (b) image corresponded to $Rh(Cl)/CeO_2$.

cubo–octahedron truncated at the (111) central plane. Therefore, the corresponding $N_t$ and $N_s$ values will be one half of those described in Ref. [23] for a complete cubo-octahedron. In accordance with this, the $N_t$ and $N_s$ values used in this work were estimated by using the following:

$$N_t = 8m^3 - (33m^2/2) + 12m - 3 \quad (2)$$

$$N_s = 15m^2 - 30m + 16 \quad (3)$$

Eq. (1) through (3) will be used as the bases for discussing our experimental results.

From the analysis of HREM micrographs like those shown in Fig. 4, corresponding to the whole series of $Rh/CeO_2$ samples, we have measured the parameter $d$ for at least 250 metal particles per catalyst. From these experimental data three different types of distribution curves were built up:

Type A: It accounts for the direct experimental data, i.e. accumulated percentage of metal particles vs. particle size ($d_k$):

$$100[\Sigma_i n_i(d_i \leq d_k)]/n_t \text{ vs. } d_k$$

Where $n_i$ is the number of metal particles with size $d_i$ and $n_t$ the total number of metal particles.

From this kind of plot, we can estimate the mean rhodium particle size, $d_m$, and, therefore a metal dispersion value ($D_d$). $D_d$ would be defined as the fraction of the total number metal atoms in a particle with the mean size, $d_m$, which are exposed at its surface:

$$D_d = N_d(Rh_s)/N_d(Rh_t)$$

Where $N_d(Rh_s)$ is the number of Rh atoms at the surface of a particle with the mean size, $d_m$ and $N_d(Rh_t)$ the total number of atoms in a particle with the mean size, $d_m$.

Type B: It plots the accumulated percentage of the total number of metal atoms contained in particles with size equal or smaller than a predefined $d_k$ value:

$$100[\Sigma_i n_i(Rh)(d_i \leq d_k)]/n_t(Rh) \text{ vs. } d_k$$

Where $n_i(Rh)$ is the number of rhodium atoms in particles with size $d_i$ and $n_t(Rh)$ the total number of metal atoms.

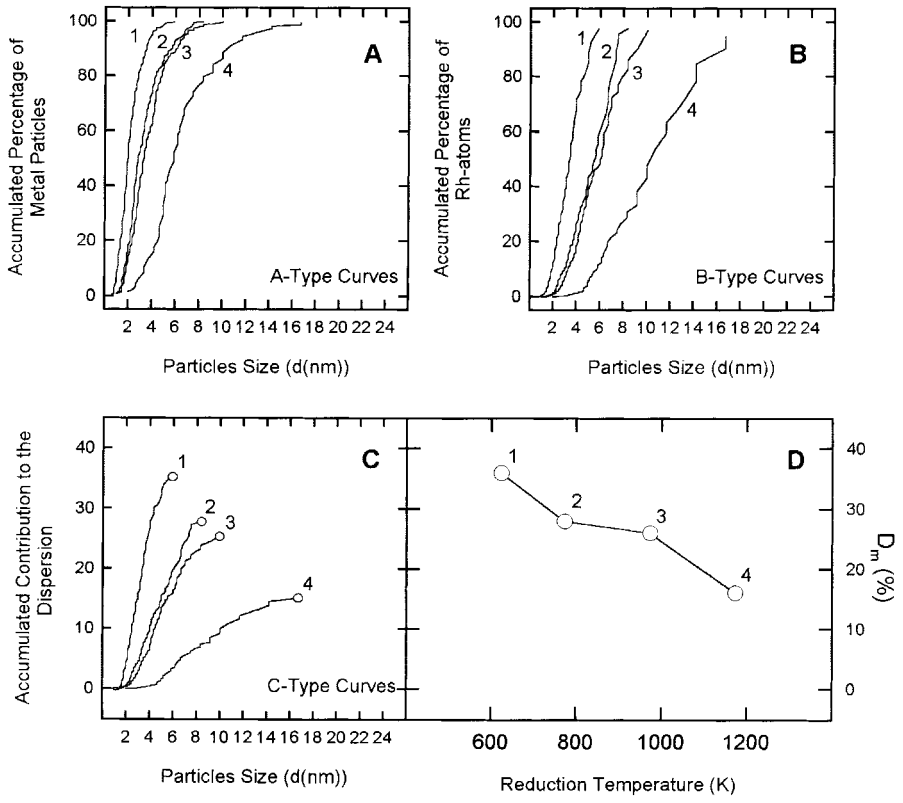


Fig. 5. Distribution curves (types A–C) corresponding to Rh(N)/$CeO_2$ catalysts reduced at 623 K (1), 773 K (2), 973 K (3) and 1173 K (4). Box D accounts for the evolution of the metal dispersion ($D_m$) as a function of $T_{redn}$.

Therefore, it would account for the mass distribution of rhodium.

Type C: It shows the fraction of the total number of rhodium atoms that are present at the surface of metal particles with size equal or smaller than a given $d_k$ value. Therefore, it would account for the contribution to the true metal dispersion ($D_m$) of the particles with a predefined $d_k$ value or smaller.

$$[\Sigma_i N_i(Rh_s)(d_i \leq d_k)]/N_t(Rh) \text{ vs. } d_k$$

Where $N_i(Rh_s)$ is the number of surface rhodium atoms in particles with size $d_i$ and $N_t(Rh)$ the total number of rhodium atoms.

Obviously, the last point of the whole distribution curve would measure the metal dispersion: $D_m = [\Sigma_i\, n_i(Rh_s)]/\, n_t(Rh)$ of the catalyst.

Fig. 5 and 6 account respectively for the distribution curves determined for our Rh(N)/$CeO_2$ and Rh(Cl)/$CeO_2$ catalysts reduced at temperatures ranging from 623–1173 K. These two figures also include a forth plot showing the evolution of $D_m$ as a function of the reduction temperature.

Some of the results obtained from the analysis of the distribution curves shown in Figs. 5 and 6 are summarized in Table 2:

There are a number of aspects to be commented on in relation to Figs. 5 and 6 as well as Table 2. First of all, it would be stated that the metal dispersions obtained from the C-type distribution curves are in good agreement with values obtained from volumetric studies of hydrogen chemisorption. Thus, in the case of the Rh(N)/$CeO_2$ catalysts the H/Rh ratios measured at 191 K after reduction at 623 K and 773 K were 0.31 and 0.27, respectively [13], these values being close to those reported in Table 2 for $D_m$. For the Rh(Cl)/$CeO_2$ catalysts a good match between the dispersion esti-

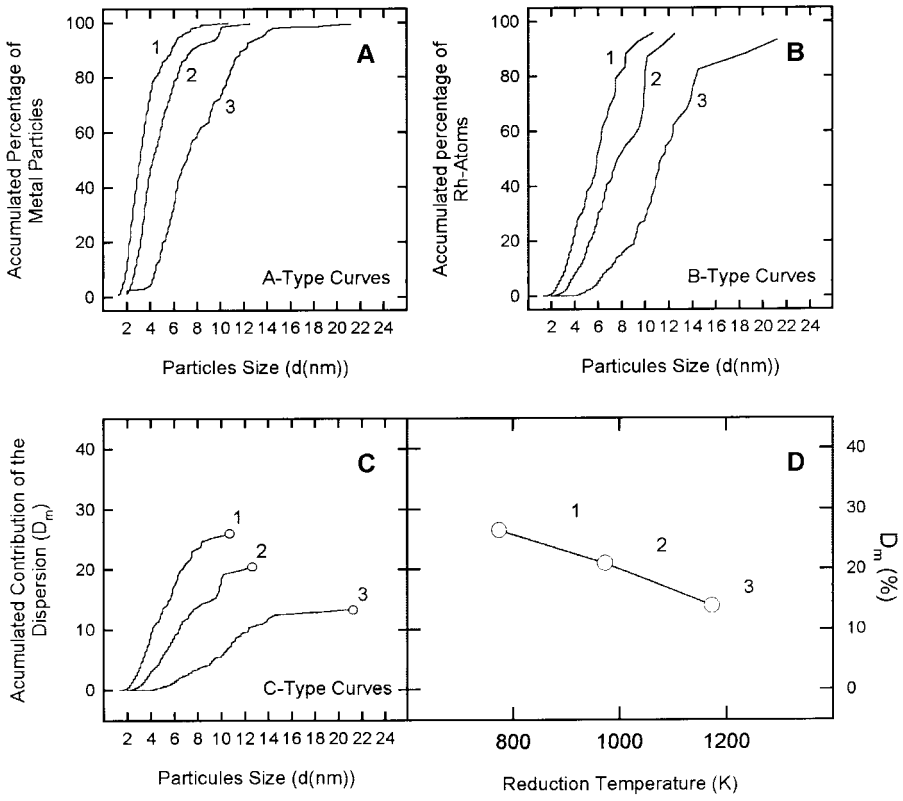


Fig. 6. Distribution curves (types A–C) corresponding to Rh(Cl)/$CeO_2$ catalysts reduced at 773 K (1), 973 K (2) and 1173 K (3). Box D accounts for the evolution of the metal dispersion ($D_m$) as a function of $T_{redn}$.

Table 2
Mean particle size and metal dispersion data ($D_d$ and $D_m$) corresponding to Rh(N)/$CeO_2$ and Rh(Cl)/$CeO_2$ catalysts reduced at temperatures ranging from 623–1173 K

| $T_{redn}$ (K) | Rh(N)/$CeO_2$ | | | Rh(Cl)/$CeO_2$ | | |
|---|---|---|---|---|---|---|
| | $d$ (nm) | $D_d$ (%) | $D_m$ (%) | $d$ (nm) | $D_d$ (%) | $D_m$ (%) |
| 623 | 2.2 | 46 | 36 | — | — | — |
| 773 | 3.3 | 38 | 28 | 3.4 | 38 | 27 |
| 973 | 3.7 | 36 | 26 | 4.8 | 29 | 21 |
| 1173 | 6.6 | 22 | 16 | 8.0 | 19 | 14 |

$d_m$: Mean particle size as determined from type A distribution curves.
$D_d$: Metal dispersion corresponding to the metal particle with the mean size ($d_m$).
$D_m$: Metal dispersion as determined from the type C distribution curves.

mated from $H_2$ isotherms at 191 K [13], H/Rh: 0.26, and that obtained from HREM work, $D_m$: 0.27, is also observed.

Focusing now on the behaviour of the different samples, it can be observed firstly that in spite of the larger metal loading of the Rh(N)/$CeO_2$ catalysts (2.5%), compared to that of the Rh(Cl)/$CeO_2$ samples (1.9%), the chlorine containing catalysts exhibit lower metal dispersions. It seems also that the latter type of catalyst are more sensitive to the reduction temperature than the former one. In any case, the highest reduction temperature applied in this work, 1173 K, induces strong sintering effects on the rhodium particles. Also worth of noting, for 973 K or higher reduction temperatures, metal sintering is accompanied by metal decoration phenomena in both (N) and (Cl) type samples [11,12].

As deduced from Table 2, $D_d$ and $D_m$ values determined for the same catalyst are significantly different from each other. This suggests that, depending on the distribution curve associated to the catalyst, the dispersion value estimated from the mean metal particle

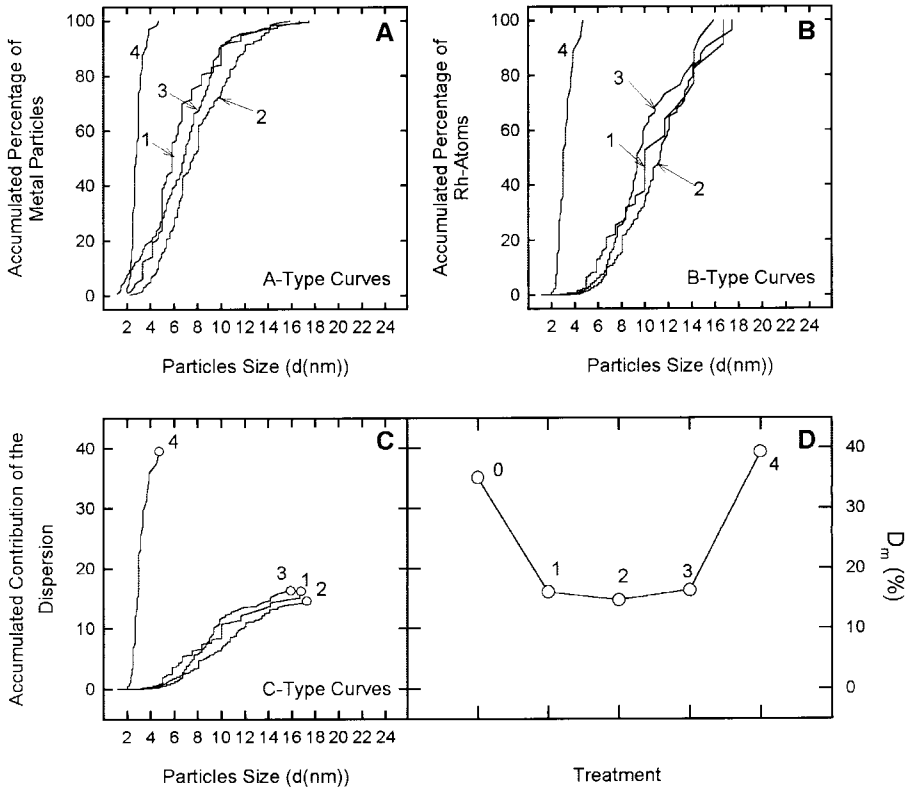


Fig. 7. Influence of the reoxidation conditions on the distribution curves (types A–C) corresponding to Rh(N)/$CeO_2$ previously reduced at 1173 K: (1) non reoxidized catalyst; (2) reoxidation at 723 K (theoretical curves for metallic Rh generated by correcting the experimental distributions for $Rh_2O_3$); (3) reoxidation at 723 K and further reduction at 623 K; (4) reoxidation at 1173 K. Box D accounts for the dispersion ($D_m$) evolution as a function of the reoxidation treatment; in case 2, $D_t$ value is used; $D_m$ for Rh(N)/$CeO_2$ catalyst reduced at 623 K (0) has also been included for comparison.

size ($D_d$) can deviate from the actual metal dispersion as determined from type C distribution curves ($D_m$). In effect, it is shown in Table 2 that in most of cases $D_d$ overestimates the true metal dispersion ($D_m$) by a 35–40%.

We have also studied the influence of the reoxidation conditions on the dispersion of our Rh/$CeO_2$ catalysts. Fig. 7 accounts for the particle size distribution curves determined upon reoxidizing the Rh(N)/$CeO_2$ catalyst previously reduced at 1173 K. Earlier $O_2$ pulses/TPO and HREM studies from our laboratory [11,12] have reported on the effect of reoxidation treatments at 373 K, 523 K, 773 K and 1173 K, on the Rh(N)/$CeO_2$ catalyst reduced at 1173 K. By digital processing of the recorded HREM images, we concluded in Refs. [11,12] that, for the lowest reoxidation temperatures, 373 K and 523 K, both metallic rhodium and the oxidized phase coexist, whereas the treatment at 773 K leads to rounded polycrystalline, probably hexagonal, $Rh_2O_3$ particles. Finally, the reoxidation at 1173 K induces the spreading of the oxidized phase over the ceria surface. In this latter case, the rhodium oxide becomes reduced under the electron beam, so that the HREM images recorded for the catalyst reoxidized at 1173 K actually consist of metal crystallites grown on ceria [11]. Fig. 7 only accounts for the fully oxidized catalysts, i.e. those treated with flowing $O_2$ at either 773 K or 1173 K.

If, as mentioned above, the phase resulting from the reoxidation treatment at 773 K consists of the so-called type I [24], hexagonal $Rh_2O_3$, the linear lattice expansion associated to the oxidation of metallic

rhodium crystallite can easily be established:

$$d(Rh_2O_3) = 1.24\, d(Rh) \quad (4)$$

Assuming that the mild reduction process of the $Rh_2O_3/CeO_2$ samples leading to $Rh/CeO_2$ does not induce sintering or redispersion of the metal, Eq. (4)) would allow us to generate the theoretical Rh size distribution curves associated to the corresponding $Rh_2O_3$ experimental distributions. From these theoretical metal distributions, specifically from the so-called type C curves, we can estimate the theoretical metal dispersion ($D_t$) associated to an oxidized catalyst. As will be discussed below, the comparison of $D_m$ for a reduced catalyst with the $D_t$ value determined from its reoxidized form, would allow us to detect the metal sintering/redispersion effects induced by the oxygen treatment.

Table 3 accounts the whole series of reoxidation studies carried out on both $Rh(N)/CeO_2$ and $Rh(Cl)/CeO_2$ catalysts reduced at either 773 K, 973 K or 1173 K.

For the lowest reoxidation temperature considered here, 773 K, $D_t$ parameter has been used to characterize the effect on the dispersion of the oxygen treatment. The dispersion values ($D_m$) for the starting reduced catalysts are also reported for comparison. Likewise, Table 3 includes the dispersion ($D_m$) values determined for the $Rh/CeO_2$ catalyst reduced at either 973 K or 1173 K, further reoxidized at 773 K and finally reduced at 623 K. Assuming that such a mild re-reduction treatment does not modify the rhodium distribution curves, the dispersion data ($D_m$) obtained from these latter experiments might well be compared with those theoretically estimated ($D_t$) from the corrected $Rh_2O_3$ size distributions.

In accordance with the results reported in Table 3, the $D_t$ values estimated for the catalysts reoxidized at 773 K are in fairly good agreement with the dispersion data ($D_m$) determined for the samples further reduced at 623 K. This observation, as well as the shape of the corresponding distribution curves included in Fig. 7, support the assumptions made above: (a) the rhodium containing phase resulting from the reoxidation treatment at 773 K actually consists of $Rh_2O_3$; and (b) the relatively mild reduction treatment at 623 K does not induce any significant modification on the rhodium distribution associated to the oxidized phase.

Also worth of commenting on, Table 3 shows that consequently to the oxidation treatment at 773 K a moderate sintering effect can always be observed, thus suggesting that the treatment above, in addition to induce the reoxidation of both metal and support would promote the growth of the oxidized rhodium particles. This effect seems to be particularly relevant in the case of the catalyst reduced at 623 K, i.e. the one showing the highest metal dispersion.

Table 3
Analysis of the rhodium particle size distribution curves resulting from the reoxidation treatments at either 773 K or 1173 K of the $Rh(N)/CeO_2$ and $Rh(Cl)/CeO_2$ catalysts reduced at 773 K, 973 K and 1173 K

| $Rh/CeO_2$ | | | | | |
|---|---|---|---|---|---|
| $T_{redn}$ (K) | Catalyst | $D_m$ | Further treatments | $D_t$ | $D_m$ |
| 623 | N | 36 | Reoxn. at 773 K | 21 | — |
| 773 | N | 28 | Reoxn. at 773 K | 23 | — |
| 973 | N | 26 | Reoxn. at 773 K | 18 | — |
| | | | Reoxn. at 773 K +Redn at 623 K | — | 18 |
| | Cl | 21 | Reoxn. at 773 K | 16 | — |
| | | | Reoxn. at 773 K +Redn. at 623 K | — | 17 |
| | | | Reoxn. at 1073 K | — | 41 |
| 1173 | N | 16 | Reoxn. at 773 K | 15 | — |
| | | | Reoxn. at 773 K +Redn. at 623 K | — | 16 |
| | | | Reoxn. at 1173 K | — | 39 |

$D_m$: Metal dispersion as determined from experimental type C distribution curves.
$D_t$: Theoretical metal dispersion as determined from converted type C distribution curves for $Rh_2O_3$ particles.

By contrast, the reoxidation treatments at the highest temperatures, 1173 K or 1073 K, which were applied to catalyst N reduced at 1173 K (Fig. 7) and catalyst Cl reduced at 973 K, respectively, have a very strong influence on the distribution curves, and consequently to this on $D_m$. In effect, as deduced from Table 3, inherent to these treatments an important metal redispersion occurs. In accordance with the increase observed in $D_m$, the corresponding distribution curves (Fig. 7), are very significantly shifted with respect to those determined for the starting catalysts reduced at either 1173 K or 973 K. Moreover, the reoxidation at 1173 K of $Rh(N)/CeO_2$ leads to a metal dispersion even larger than that of the original catalyst directly reduced at 623 K, the lowest reduction temperature investigated here.

To summarize, we have studied the influence of the reduction/ reoxidation treatments applied in a wide range of thermal conditions (623–1173 K) on the particle size distribution and metal dispersion of a series of $Rh/CeO_2$ catalysts. From our investigation, a number of conclusions would be outlined. In spite of some earlier suggestions from the literature [25–27], this work, like several others recently appeared [8–15] clearly show that HREM is an extremely useful technique for investigating ceria supported noble metal catalysts. Moreover, the combination of both experimental and computer simulation techniques strengthens very much the intrinsic capabilities of HREM. Image calculations, in effect, have helped us in a number of important ways: (a) to establish reasonable detection limits for rhodium particles grown on a heavy metal oxide like ceria; (b) to define the model rhodium particle to be used as the basis for analysing our experimental results; (c) to be more confident about the rhodium particle size measurements carried out on both profile and planar projection experimental images.

Also worth of noting, our study shows that reduction treatments up to 973 K induce a moderate, though significant, decrease of $D_m$, the effect being larger when chlorine is present. By contrast, the reduction at 1173 K leads to strong rhodium sintering. Regarding the effect of the reoxidation treatments, strong redispersion could only be observed at the highest range of temperatures 1073–1173 K, whereas reoxidation at 773 K induces rhodium sintering. Finally, the analysis of the different distribution curves reported here indicates that metal dispersions estimated from type A distributions, i.e. from the mean particle size value ($D_d$), can significantly disagree from that, more accurate, determined from type C curves, $D_m$. All these data can be relevant in connection with deactivation/ regeneration mechanisms operating in ceria supported noble metal catalysts, and by extent in TWC's.

## Acknowledgements

This work has been supported by the DGICYT (Project PB95-1257), the CICYT (Project MAT96-0931), and the Junta de Andalucía. We acknowledge JM for a loan of precious metals. The HREM images reported in this work were obtained at the Electron Microscopy Facilities of the University of Cádiz.

## References

[1] S.E. Golunski, H.A. Hatcher, R.R. Rajaram, y T.J. Truex, Appl. Catal. B: Environmental 5 (1995) 367.
[2] G.S. Zafiris, R.J. Gorte, J. Catal 139 (1993) 561.
[3] P. Meriaudeau, M. Dufaux, C. Naccache, Stud. Surf. Sci. Catal. 11 (1982) 95.
[4] J. Barrault, A. Alouche, V. Paul-Boncour, L. Hilaire, A. Percheron Guegan, Appl. Catal. 46 (1989) 269.
[5] J. Cunningham, D. Cullinane, J. Sanz, J.M. Rojo, J.A. Soria, J.L.G. Fierro, J. Chem. Soc. Faraday Trans. 88 (1992) 3233.
[6] A. Trovarelli, G. Dolcetti, C. Leitenburg, J. Kaspar, P. Finetti, A. Santoni, J. Chem. Soc. Faraday Trans. 88 (1992) 1311.
[7] C. Binet, A. Jadi, J.C. Lavalley, M. Boutonet-Kizling, J. Chem. Soc. Faraday Trans. 88 (1992) 2079.
[8] H.D. Cochrane, J.L. Hutchinson, D. White, G.M. Parkinson, C. Dupas, A.J. Scott, Ultramicroscopy 34 (1990) 10.
[9] M. Pan, Ph. D. Thesis, Arizona State University (1991).
[10] A.K. Datye, D.S. Kalakkad, M.H. Yao, y.D.J. Smith, J. Catal. 155 (1995) 148.
[11] S. Bernal, F.J. Botana, J.J. Calvino, G.A. Cifredo, J.A. Pérez Omil, y J.M. Pintado, Catal. Today 28 (1995) 219.
[12] S. Bernal, G. Blanco, J.J. Calvino, G.A. Cifredo, J.M. Gatica, J.A. Pérez, J.M. Pintado, Stud. Surf. Sci. Catal. 82 (1994) 507.
[13] S. Bernal, F.J. Botana, J.J. Calvino, M.A. Cauqui, G.A. Cifredo, A. Jobacho, y J.M. Pintado, J.M. Rodríguez-Izquierdo, J. Phys. Chem. 97 (1993) 4118.
[14] S. Bernal, J.J. Calvino, M.A. Cauqui, G.A. Cifredo, A. Jobachoy, y J.M. Rodríguez-Izquierdo, Appl. Catal. 99 (1993) 1.
[15] S. Bernal, F.J. Botana, R. García, Z. Kang, M.L. López, M. Pan, F. Ramírez, J.M. Rodríguez-Izquierdo, Catal. Today 2 (1988) 653.
[16] B.J. Cooper, Platinum Met. Rev. 38 (1994) 2.

[17] D.D. Beck, C.J. Carr, J. Catal 144 (1993) 296.
[18] S. Bernal, G.A. Cifredo, J.J. Calvino, J.M. Rodríguez-Izquierdo, V. Perrichon, A. Laachir, J. Catal. 137 (1992) 1.
[19] S. Bernal, J.J. Calvino, G.A. Cifredo, A. Laachir, V. Perrichon, J.M. Herrmann, Langmuir 10 (1994) 717.
[20] J.A. Pérez Omil, Ph. D. Thesis, University of Cádiz (1994).
[21] M. Flueli, Ph. D. Thesis, Ecole Politechnique Federale de Laussane (1989).
[22] V. Radmilovic, M.A. O'Keefe, Proc. MSA, 53 (1995) 564.
[23] R. Van Hardeveld, F. Hartog, Surf. Sci. 15 (1969) 189.
[24] A. Wold, K. Dwight, Solid State Chemistry, p. 117, Chapman and Hall, New York (1993).
[25] M. Primet, M. El Azhar, R. Frety, M. Guenin, Appl. Catal. 59 (1990) 153.
[26] J.L. Duplan, H. Praliaud, Appl. Catal. 67 (1991) 325.
[27] A.T. Ashcroft, A.K. Cheetham, P.J.F. Harris, R.H. Jones, S. Natarajam, G. Sankar, N.J. Stedman, J.M. Thomas, Catal. Lett. 24 (1994) 47.